Eur. Phys. J. E **15**, 53–60 (2004)
DOI 10.1140/epje/i2004-10036-x

THE EUROPEAN PHYSICAL JOURNAL E

Quantitative description of foam drainage: Transitions with surface mobility

A. Saint-Jalmes[a], Y. Zhang[b], and D. Langevin

Laboratoire de Physique des Solides, Université Paris-Sud, 91405 Orsay, France

Received 29 April 2004 /
Published online: 21 September 2004 –

Abstract. We have performed forced drainage experiments on aqueous foams of bubble diameters D varying from 0.18 to 8 mm, and made with different surfactant and protein solutions (providing different surface viscoelastic properties). Changing bubble size or surface properties allows to evolve between two drainage regimes, the respective dimensionless permeabilities also varying with these parameters. We show that the bubble size and surface properties can be incorporated into a single surface mobility parameter that controls the transition between the two drainage regimes. The permeability measurements indicate how do the hydrodynamic resistances of the foam channels and nodes depend on surface mobility. Taking advantage of the large range of experimental conditions, leading to a variation of the mobility parameter over more than 3 decades, a simple and consistent description of both the drainage regimes and the transition in between them is obtained. For the smallest bubbles ($D < 0.5$ mm) anomalous behaviors are observed and discussed.

PACS. 82.70.Rr Aerosols and foams – 47.60.+i Flows in ducts, channels, nozzles, and conduits – 47.55.Mh Flows through porous media

1 Introduction

An aqueous foam is a dispersion of a gas into a liquid, in the presence of surfactant molecules stabilizing the air-liquid interfaces [1]. Despite the presence of surfactants, the stability of aqueous foams is limited, as they always collapse after a certain time and vanish. Among the different destabilizing effects occurring during a foam lifetime, the gravitational drainage is probably the most critical one, as it changes irreversibly the foam liquid content. Due to gravity the liquid flows through a foam and accumulates at its bottom, leading to a drier and more fragile foam, for which other destabilizing effects such as coarsening and film rupture are more effective. Liquid content variations also lead to changes of the foam mechanical, optical and electrical macroscopic properties [1]. Regarding the foam applications, one might want to make stable foams, to avoid them, or to optimize one of their properties: in all these cases, knowing how do the foams drain is always an important issue.

In the last ten years, foam drainage has been a very active field, both theoretically and experimentally [1–31], complementing the earliest works [32–34]. Two different drainage regimes have been observed, at the macroscopic scale [2,8–10], as well as at the scale of a single foam channel [22,30,31], and related to opposite limits of the bubble surface viscoelasticity. A first regime has been associated to the limit of rigid and solid-like surfaces, and the other one to mobile fluid-like surfaces. In both of these extreme cases, comparisons between data and drainage models have shown that, for rigid surfaces, the main hydrodynamic dissipation is within the foam liquid channels (the Plateau Borders, PBs) where the flow is Poiseuille-like [3,5,14]; on the other hand, for mobile surfaces, the flow in the PBs is more plug-like, so that the main viscous dissipation is within the nodes (the junction of four PBs) [8,11]. All the models are based on the same ingredients, they consider the foam as a porous medium with the liquid flowing in the network of PBs interconnected at the nodes. However, the foam is a particular porous medium since the PBs and nodes sizes depend on the liquid content, so that the permeability is not constant and is directly coupled to the foam liquid content. In these models, the macroscopic drainage behavior is finally inferred from microscopic flow descriptions at the scale of the elementary structure (a PB, connected to a node).

Nevertheless, many questions remain unsolved regarding a complete quantitative picture. The models only describe the extreme cases of surface mobility. The corresponding features have been observed experimentally, but it is still not clear which precise conditions and foam

[a] e-mail: saint-jalmes@lps.u-psud.fr
[b] *Present address*: Department of Chemistry and Biochemistry, The Florida State University, Tallahassee, FL, USA.

parameters are associated to each limit. The surface rheological properties appear to be important, but they are described by several different parameters and it is not yet clear which one is the most important in the drainage problem. It also seems that other foam parameters play a role in the selection of the flow regime, especially the bubble size and the liquid fraction. Leonard and Lemlich modeled the flow in a single PB and took into account the coupling between the flow in the bulk and at the surface. They introduced a simple "mobility parameter", incorporating the PB size, the bulk and surface shear viscosity. This parameter, describing the flow in PBs (from Poiseuille like to plug-like one), may possibly be also relevant for the transition between the macroscopic drainage regimes [32]. This description in terms of surface mobility parameter and the coupling between surface and bulk flow in a PB have recently been studied in more details by numerical simulations [35–37], but these ideas have not yet really been quantitatively tested over a large range of experimental conditions. Moreover, quantifying the surface mobility should also help to understand and describe the drainage properties between the two extreme limits.

The quantitative aspects are obviously also important. The values of the dimensionless permeability constants, appearing in the drainage speed, have to be measured, and their dependence with the experimental conditions identified. Indeed, experimentally and especially in the limits of mobile surfaces, different values for a same permeability constant have been measured, but for different bubble sizes [11,23,27]. Predictions of these permeability values, and of their relations to the hydrodynamic resistances of each foam structures (PBs and nodes), strongly rely on models for the PBs and node geometry. So, the comparisons with measurements can ultimately help to check the validity of both these geometrical descriptions and constants, and of the drainage models assumptions. An important related issue is then to finally identify to which level of refinement one must describe the foam structure to explain the drainage properties, and what is the effective role of each elements of the foam. Finally, it is also important to determine, regarding the application foreseen (from long-lasting foams to fast-drainage ones), which are the most efficient foam parameters to tune the timelife of any foam.

In this paper, we first recall the theoretical background (models for the different limits of surface properties and introduction of the surface mobility parameter), together with a possible approach to model the intermediate regime. We then present new results of forced drainage experiments, where we have widely changed the bubble diameter (by almost a factor 50), and the surface properties (by using different surface-active molecules). We then show that for a large range of experimental conditions, a coherent picture can be established.

2 Materials and setup

Most foams were made by the bubbling method, and the turbulent mixing method was used to obtain the smallest bubbles (diameter $D = 0.18$ mm) [7]. In the bubbling method, the gas is injected inside the solution through porous cylinders made of fritted glass. In order to change the bubble size, different frit porosities (0 to 4) were used (providing intermediate diameters, up to 3.5 mm). The largest bubbles (diameter D from 4 mm to 8 mm) were made with perforated homemade plugs. The bubble size has thus be changed by almost a factor 50.

Sodium Dodecyl Sulfate (SDS) of high purity, dodecanol and casein (milk protein) were purchased from Sigma. Typical concentrations were: 10 g/L for SDS, 0.1 g/L for dodecanol, and 1.5 g/L for casein. All the solutions were made with ultra-pure Milli-Q water. The casein solution is made in a phosphate buffer in order to fix the pH at 5.6. We measured the rheological properties of all the solutions: the viscosities are equal to the one of water for the surfactant solution, and 10% higher for the casein solution. In order to produce the foam, we used either a pure fluorinated gas (C_2F_6), or nitrogen loaded with C_6F_{14} vapor traces, to strongly reduce the coarsening rates [38].

We performed forced drainage experiments, easier to analyze than the free drainage experiments where long experimental times are needed, and interpretation is more difficult (problem with the initial vertical foam uniformity, and with boundary conditions at the foam bottom). In a forced drainage experiment, the foam is first allowed to drain completely. This provides a reproducible and controlled initial stage. Then, the surfactant solution is injected at the top of the foam sample at a controlled flow rate: due to gravity and capillarity, a liquid front propagates downward in the foam at a constant velocity v, leaving a constant liquid fraction ε above it. Results are expressed via power law relationships between v and Q (or ε): $v \sim Q^{\alpha}$ (meaning also $v \sim \varepsilon^{\beta}$ with $\beta = \alpha/(1-\alpha)$ as the liquid volume conservation implies $Q/S = \varepsilon v$, with S being the sample cross-section).

To localize the front and to measure its velocity, we used a multiple light scattering technique in transmission (analogous to the Diffusive Transmission Spectroscopy, DTS [39]). In the multiple scattering regime, the light transmission intensity I_t is simply related to the foam liquid fraction: in a first approximation, it is inversely proportional to $\sqrt{\varepsilon}$ [40]. This means that qualitatively a wet foam will transmit less light than a dryer one. One can then easily detect differences in liquid fraction, like drainage fronts, and their spatial and temporal evolution with a CCD camera on one side of the sample, and a white light illumination on the other [23]. This technique is very simple and well adapted for measuring drainage front velocities. It is also non intrusive as no additives or probes within the sample are needed. As it based on the random walk of photons through the foam, it is also clear that artifacts at the wall are not important. In order to accurately visualize the front, the only requirement is that the foam must be thick enough to get enough scattering events. Even if the asymptotic multiple scattering regime is not completely obtained with a sample thickness of typically 10 bubbles [39,40], it is already sufficient to

detect differences in the transmitted intensity above and below the front. We used foam cells having parallelepiped shapes, with the same height (70 cm), but different width and thickness t depending on bubble size ($t > 10D$). The width of the cells was kept equal to $6t$ in order to minimize the photon leaks by the sides of the cells, and to mimic an ideally infinite width. The front was followed over at least 25 cm, and its precise position determined by image treatment using a computer software developed by IT-Concept. We verified the agreement between the DTS measurements and those made by conductimetry measurements with electrode arrays along the height of the drainage cell. The resolution of light scattering technique is higher, allowing for instance to evidence the non-symmetrical shape of the front.

3 Drainage models and definitions

A foam drainage equation describes the time and space evolution of the foam liquid fraction $\varepsilon(z,t)$. It predicts for instance the relation between the front speed v and the flow rate Q in a forced drainage experiment. All the models are based on the local description of the flow in a single foam structural element (a PB and a node). The drainage equation is obtained by averaging over the whole network of PBs and nodes, neglecting the thin films. This last assumption appears quite reasonable as the liquid within the foam is almost only distributed within the PBs. In the limit of low liquid fractions one can write: $\varepsilon \approx \delta \frac{r^2}{L^2}$, where L is the PB length, r its radius of curvature, and $\delta = 0.17$ [11]. In the following, the bubbles are replaced by Kelvin cells (tetrakaidecahedra), for which $D = cL$, with $c \approx 2.7$ [11].

When the velocity is zero at the surface of the PBs (rigid surfaces), the flow inside the PBs is Poiseuille-like. In the forced drainage mode, the model leads to a front velocity such as [2–4]

$$v = K_{\rm c}^0 \frac{\rho g L^2}{\mu}\varepsilon = \left(K_{\rm c}^0 \frac{\rho g L^2}{\mu}\right)^{1/2} (Q/S)^{1/2}, \qquad (1)$$

where ρ is the liquid density, g is the gravitational acceleration, μ is the liquid bulk viscosity and $K_{\rm c}^0$ a dimensionless permeability. Following [11], we introduce a dimensionless resistance $R_{\rm c}^0$, such as: $R_{\rm c}^0 = 1/(3\delta K_{\rm c}^0) = A/K_{\rm c}^0$, and $A \approx 2$. $K_{\rm c}^0$ is related to the peculiar shape of the PB cross-section, and the calculation gives: $K_{\rm c}^0 = 6.610^{-3}$ and $R_{\rm c}^0 = 290$ [2–4].

Leonard and Lemlich [32] considered the flow in a single PB when the surfaces are not completely rigid, and analyzed the coupling between bulk and surface flows. Considering that the three corners of the PB are fixed, as they are connected to the thin films, tangential shears can then occur within the surfaces. They introduced the surface shear viscosity $\mu_{\rm s}$ and described the coupling with the parameter $M = \frac{\mu r}{\mu_{\rm s}}$, (this parameter was also used later by Kraynik [33]). Note also that M is the inverse of the Boussinesq number. Introducing the bubble diameter in M, and in the limit of low liquid fraction ($r = L\sqrt{\varepsilon/\delta}$), the parameter M can be written as: $M = \frac{\mu r}{\mu_{\rm s}} = \chi \frac{\mu D\sqrt{\varepsilon}}{\mu_{\rm s}}$, with $\chi = 1/(c\sqrt{\delta}) \approx 0.9$. For low values of M (high surface viscosity, for instance), the coupling and surface mobility are small, and the flow remains Poiseuille-like. Deviations appear as soon as M is close to 0.1 [32,35,36]. Slightly different forms for the correction have been found in the numerical calculations [32,35,36]. For the purpose of this paper, we have simplified these different results by simpler forms, fitting their predicted curves from low M up to $M = 10$. The front velocity can then be written:

$$v = \frac{\rho g L^2}{\mu} K_{\rm c}^0 (1 + a M^b)\varepsilon = \frac{\rho g L^2}{\mu} K_{\rm c}^0 \left(1 + a\left(\frac{\chi \mu D\sqrt{\varepsilon}}{\mu_{\rm s}}\right)^b\right)\varepsilon, \qquad (2)$$

with $a = 1.55$ and $b = 0.75$ for the expression given in [32, 35], and $a = 2.4$ and $b = 1$ for the expression given in [36]. We will use these two sets of numerical results for a and b later in our data analysis. It turns out that this correction has only small effects on the exponent α (or β), which remains always close to 1/2 (or 1). In fact, α can only increases up to 0.6 for very large M values. The main effect of this correction is on the prefactor of the power law curve: it increases significantly with M, meaning that when the surfaces become more mobile, the hydrodynamic resistance of the PBs decreases.

Another coupling has been proposed between the PB bulk and surface flow, due to surface tension gradients [21]. This coupling can be described by a second mobility parameter $N = \frac{\mu D_{\rm eff}}{Er}$, where $D_{\rm eff}$ is an effective surface diffusion coefficient, and E the Gibbs elastic modulus of the surface. If N is small, there is no surface flow and $\alpha = 0.5$. If N is large, surface flow is important, and it has been predicted that the exponent α for forced drainage is equal to 1/3. However, for this coupling, predictions for intermediate N (such as Eq. (2) for M) are not available. Note that the variations of M and N with bubble size are opposite.

In the limit of very mobile surfaces (large M or N), the flow is plug-like in the PBs, and it has been proposed that the dissipation in the node becomes then predominant. In that case, the front velocity is given by [8,11]

$$v = K_{\rm n}^0 \frac{\rho g L^2}{\mu}\varepsilon^{1/2} = \left(K_{\rm n}^0 \frac{\rho g L^2}{\mu}\right)^{2/3} (Q/S)^{1/3}. \qquad (3)$$

One can also define a dimensionless node resistance $R_{\rm n}^0$, equal to: $R_{\rm n}^0 = (2\delta_a)/(3\sqrt{\delta}\delta_{\rm n} K_{\rm n}^0) = B/K_{\rm n}^0$, where δ_a is the constant relating a PB cross-section to its radius of curvature ($\delta_a = 0.161$) and $\delta_{\rm n}$ the constant relating the node volume to this same radius of curvature ($\delta_{\rm n} = 0.31$) [11]. With these values $B \approx 0.9$. The prediction of the value of $K_{\rm n}^0$ relies on complex numerical simulations. It has been proposed that $K_{\rm n}^0$ should be close to $K_{\rm c}^0$ [18,41], but no clear demonstration has been given yet. Also, no complete description of the intermediate regimes of surface mobility in the nodes (using M or N) exists yet. In the limit of low surface mobility, the nodes can be considered as small complementary parts of PBs, leading to corrections in the PB effective length [18].

The previous models described the drainage in the limits of low or high surface mobilities. For the intermediate regime, and following the previous approaches in terms of PB and node hydrodynamic resistances, it has been proposed to consider that PBs and nodes are resistors mounted in series, whose resistances depend on the mobility parameters M and/or N [29]. In the case of forced drainage, one could then write

$$v = \frac{\rho g L^2}{\mu}\varepsilon\left(\frac{1}{1/K_{\rm c}(M,N) + \sqrt{\varepsilon}/K_{\rm n}(M,N)}\right) = \frac{\rho g L^2}{\mu}\varepsilon\left(\frac{1}{(1/A)R_{\rm c}(M,N) + (1/B)\sqrt{\varepsilon}R_{\rm n}(M,N)}\right). \quad (4)$$

The remaining issue is then to determine the dependence of the resistances or permeabilities with surface mobility, first validating then extending equation (2) that only predict the variation of $K_{\rm c}$ with M. Equation (4) is consistent with the two previous limits: for low surface mobility (low M or N), the PBs resistance should be the largest ($K_{\rm c} \ll K_{\rm n}$), and one recovers equation (1); for high surface mobility, $K_{\rm c} \gg K_{\rm n}$ and equation (3) is recovered. This equation allows to correctly analyze the forced drainage data in the intermediate regime (where power law adjustments with a single exponent, like $v \sim \varepsilon^{\beta} \sim Q^{\alpha}$, would have given $1/2 < \beta < 1$ and $1/3 < \alpha < 1/2$).

It is important to recall that all these models rely on several assumptions. The first one is that the liquid flows only through the PB-node network, and that the liquid volume in the thin films between bubbles remains negligible and play no role in the liquid transport. Leonard and Lemlich showed that the films play however an important role in the PB boundary conditions: they maintain the velocity of the three corners of a PB equal to zero. Observations of closed liquid circulations within the thin films show that there is often an upward liquid flow in the vicinity of the PB. Since the liquid moves downward in the PB, there must be a point between films and PBs where the velocity is zero. However, the exact description of the film/PB connections, where pinching effects also occur [42], still need to be completely clarified. The second important assumption in these models is that they are in principle only valid in the limit of low liquid fraction (volume of the nodes small compared to the one of the PBs). It is thus important to check experimentally the validity of these models by varying the foam liquid fraction.

4 Forced drainage experiments

In forced drainage experiments, one can study the variation of the front velocity v with the flow rate Q of the injected fluid; v is usually plotted *versus* Q/S which has also the dimension of a velocity. Figure 1a presents forced drainage curves for foams made with a SDS solution at different bubble diameters D, ranging from 0.18 mm to 8 mm (the arrow points toward larger D). Figure 1b presents the curves for the same range of diameters for the casein solution. Similar curves were obtained for the SDS-dodecanol solutions (but for a smaller range of diameters).

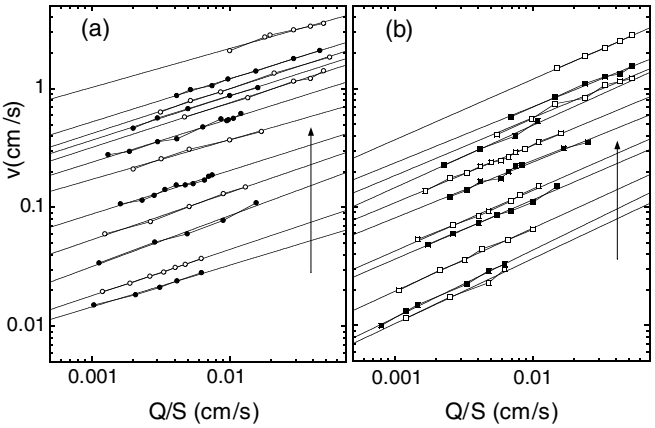

Fig. 1. Forced drainage curves at different bubble diameters, ranging from 0.18 mm to 8 mm (the arrows indicate the increase of diameter): (a) SDS foams and (b) casein foams. The data are fitted with power laws. In each graph, alternative empty and full symbols are just used to enhance the differences between the successive curves.

For a given Q/S, the smallest velocities correspond to the smallest bubble diameter. This corresponds also to the highest liquid fraction observed above the front, rising up to 25%. Larger bubbles lead to larger drainage velocities, and smaller liquid fractions, typically between 1 to 10%. Note that we have been able to measure drainage velocities ranging over more than 2 decades. The maximum injection rate and subsequent liquid fraction is determined by the occurrence of a convective instability [43,44], above which bubbles start to move, and no drainage front can be observed. The corresponding liquid fraction threshold decreases with increasing the bubble size.

The data show that, for given bubble size and Q/S, the drainage velocities are always larger for SDS solutions than for protein solutions. The difference is more important for the small Q/S. At large Q/S the velocities become closer and almost equal when the maximum liquid fraction is attained (just before the convective instability [43, 44]). The curves of Figure 1a and 1b can be fitted to power laws, and the variation of the corresponding exponents α with bubble diameter are reported in Figure 2. For the protein foams, α is always close to 1/2, consistent with the rigid surfaces models (Eq. (1)): interfaces covered by proteins are indeed expected to be very rigid, as proteins are irreversibly adsorbed and form gel-like structures. For SDS foams, where the bubble surfaces are expected to be fluid-like, we find a more complex behavior: α is consistent with the model of mobile surfaces for small and large bubbles, but in between (around $D = 1$ mm) α increases up to 0.4. This type of intermediate behavior is also seen for the SDS/DOH foams: α varies between 1/3 and 1/2, but the values are larger than for SDS foams at a given bubble size (Fig. 2). SDS/DOH monolayers at the film surfaces are expected to be more rigid than SDS ones, as the DOH molecules can fill the gaps in between the SDS ones, and then increase the surface compacity. So, there is a relatively good correlation between the measured α and

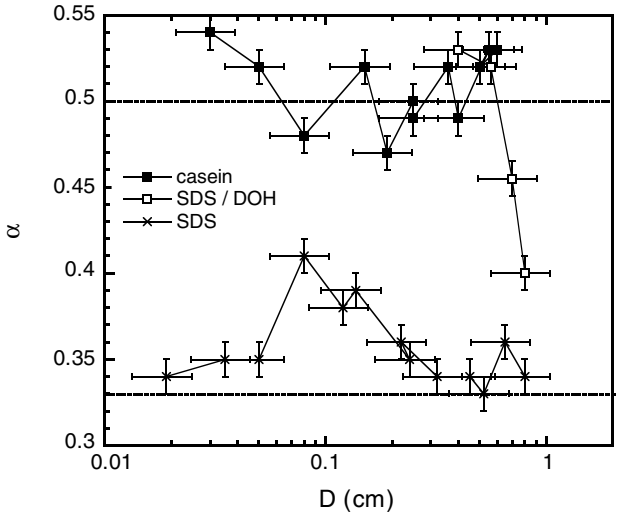

Fig. 2. Exponents α of the power law fits as a function of bubble diameter, for SDS (crosses), SDS/DOH (white squares) and casein foams (black squares). The two horizontal lines corresponds to the theoretical values 1/2 and 1/3 (Eqs. (1) and (3)).

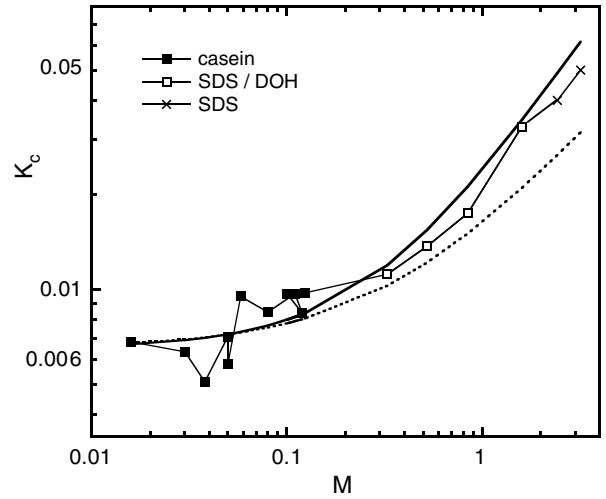

Fig. 3. Dimensionless permeability K_c as a function of the mobility M. The solid and dashed lines represent, respectively, the models of [32] and [36]. The surface shear viscosity μ_s of each solution is adjusted in order to fit with the two models. Crosses are for SDS foams, white squares for SDS/DOH foams, and black squares for the casein foams.

the surface properties, but the results also show that the drainage regime depends on the bubble size.

Within a given drainage regime, the drainage velocity depends on the bubble size. We have extracted the permeabilities K_c and K_n by fitting the data with equations (1) and (3) in the cases where α is close to 1/2 or 1/3, respectively (in practice, we fixed $\alpha = 0.5$ or 0.34 in order to obtain the permeabilities). For the intermediate cases ($\alpha \approx 0.4$), we used equation (4) to extract a (K_c, K_n) couple for each curve. It turns out that both K_c and K_n are not constant, and depend strongly on the surface properties and on the bubble size.

5 Interpretation and discussion

We have first compared the K_c values with the predictions of the model from Leonard and Lemlich (Eq. (2)), predicting the variation of K_c with M (*i.e.* with D, μ, μ_s and ε). The volume fraction ε depends on the flow rate, and is not constant along a drainage curve $v(Q)$. The value determined for K_c by fitting the curve with equation (1) is therefore an average over a range of ε, and thus also a range of M. In order to ascribe a single value of M to each measurement, we have replaced the range of ε encountered by its mean value ε_m: $M = \frac{\chi\mu D\sqrt{\varepsilon}}{\mu_s} \approx \frac{\chi\mu D\sqrt{\varepsilon_m}}{\mu_s}$. This simplification looks reasonable: i) as already said, taking into account the corrections due to M (Eq. (2)) does not significantly change the power law exponent α ($v \sim \varepsilon^1 \sim Q^{1/2}$), ii) $\sqrt{\varepsilon}$ changes only slightly with Q along an experimental curve, and iii) the variations of M due to variations of D and surface properties are much larger than those due to ε. With this approximation, the Leonard and Lemlich correction (Eq. (2)) is reduced to a change of the permeability in the equation (1), $K_c = K_c^0(1 + aM^b)$. The surface shear viscosities of the solutions used could not be measured and were treated as adjustable parameters, in order to find agreement between K_c measurements and the predictions of [32] and [36] (in practice, each solutions data set is independently adjusted to a virtually ideal curve in between the two slightly different predicted ones). It is actually possible to find a set of surface viscosities ($\mu_s = 10^{-2}\,\mathrm{g/s} = 10^{-5}\,\mathrm{Pa\cdot s\cdot m}$ for the casein solution, $\mu_s = 1.8\cdot10^{-3}\,\mathrm{g/s} = 1.8\cdot10^{-6}\,\mathrm{Pa\cdot s\cdot m}$ for the SDS/DOH solutions, and $\mu_s = 8\cdot10^{-5}\,\mathrm{g/s} = 8\cdot10^{-8}\,\mathrm{Pa\cdot s\cdot m}$ for the pure SDS solutions) for which all the permeabilities, once plotted as a function of M, get rearranged and sorted along a single continuous curve, in agreement with the predictions (see Fig. 3). It turns out that these surface viscosities are in good agreement with previous measurements [45] and with similar estimations at the scale of a single PB [30,31]. So, the observed increase of K_c is therefore likely due to the bulk/surface coupling described by the parameter M. This means also that, quite unexpectedly, drainage experiments can be a valuable method to determine shear viscosities (by quantifying the shift from pure Poiseuille flows in the PBs). The value found for small M is in good agreement with the theoretical prediction K_c^0, confirming that the limit of rigid surfaces is now well understood.

Using the previously determined values of μ_s, we can now plot and summarize all the results obtained for various bubble sizes and surface properties as a function of M only (Fig. 4). Note that we are covering more than 3 orders of magnitude in M. Figure 4a represents the evolution of α with M. As for the permeability K_c, the data from the different solutions, follow now a single curve over the whole range of M. This curve shows two well-defined drainage regimes for small and large M, which are interpreted as regimes controlled either by the dissipation in the PBs or in the nodes, respectively, and an intermediate transition regime in between them, for $0.8 < M < 3.5$. M appears thus to be, over a very large range of experimental

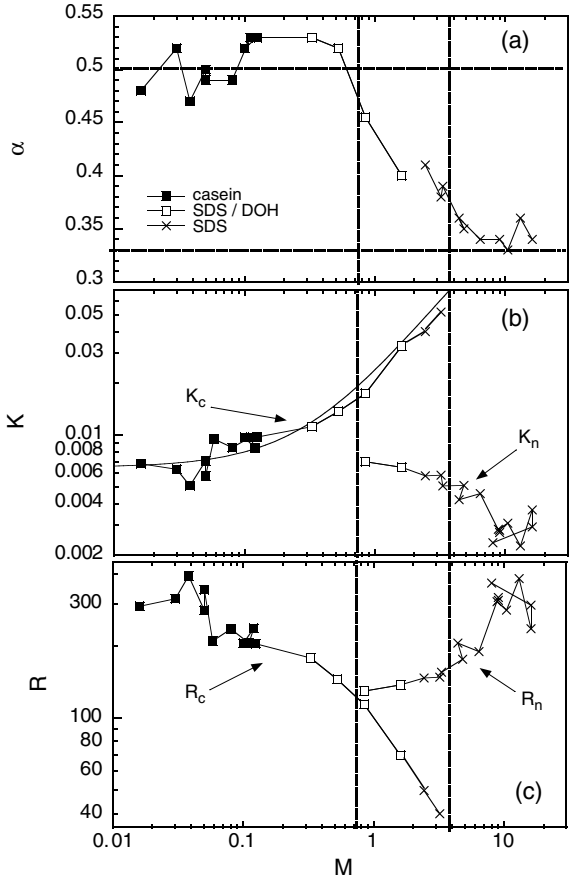

Fig. 4. Surface mobility dependence of the exponent α (a), permeabilities K_c and K_n (b), and hydrodynamic resistances R_c and R_n (c). The dashed lines indicate the transition range for α (in a), corresponding well to the crossover of the resistances (in c). The solid curve in (b) is after the model of [36].

conditions, the pertinent control parameter to determine the actual type of drainage.

The parameter M depends also on the liquid fraction ($M \sim \sqrt{\varepsilon}$); so, variations of only ε could then induce drainage transitions, for constant D and surface properties. Theoretically, in a single forced drainage experiment, the different regimes and the transition should thus be found as Q is varied (meaning that the exponent α could change from 1/2 to 1/3 along a curve). However, in experiments, the variation of ε is too small to detect changes of α.

In Figure 4b, we present together the values of K_n and K_c. We have found that K_n remains always smaller than K_c, and depends only slightly on M. There is a good continuity between the values of K_c, K_n obtained in the intermediate regime with equation (4) and those obtained directly in the pure rigid or mobile surface regimes. This result validates therefore the model of hydrodynamic resistance in series and the analysis of the intermediate regime.

The permeabilities K_c and K_n are useful to describe the drainage velocity. However, for a better understanding of the drainage regimes, the resistances R_c and R_n are the important quantities to be compared, as they represents the actual contributions of the PBs and nodes, once normalized by their geometrical aspects. In Figure 4c, the hydrodynamic resistances of the PBs and nodes, calculated from the permeabilities, are plotted *versus* M. When M increases, the coupling between bulk and surface flow in the PBs increases, and the surfaces loose their ability to resist to the flow: the PB resistance decreases, according to the Lemlich model. The flow in a PB is no longer Poiseuille flow, the velocity is non-zero at the surface, but the corners remain immobile, permitting the foam structure to be stable. The drainage regime remains controlled by the PBs, up to the point where their resistance become smaller than the resistance of the nodes. We have found that there is a crossover range where the PB and node contributions are actually equivalent. For larger M, the drainage is controlled by the dissipation in the nodes, which slightly increases with M.

An important result is the consistency between the drainage regime transition range (deduced from the drainage curve exponent α, Fig. 4a), and the PB and node resistances crossover range (deduced from the drainage curve prefactors, Fig. 4c). We have found that the transition range seen in Figure 4a corresponds precisely to the one seen in Figure 4c, where the PB and node resistances are equal, and cross each other. More precisely, in the transition range, R_n is somewhat larger than R_c, and this is consistent with equating hydrodynamic contributions of the nodes and PBs in equation (4). Such an agreement between the measurements validates our global interpretation of these drainage regimes, as well as the description of the PBs and node geometries (via the numerical constants A and B used in the calculations of R_c and R_n).

The theoretical values of K_n (R_n) and their dependence on M are not known, because the shape of the node and the flow inside are quite complex to model for all the surface mobilities. However, our results are in agreement with recent simulations tending to show that K_n should be of the same order as K_c [18,41] and that R_n should increase with M. Further theoretical work is in progress on these issues, and complete comparisons with the data should be soon possible. It is interesting to note that in the two extreme limits, our results show that R_c and R_n are almost equal. Experimentally, in the limit of very mobile surfaces, the values obtained here for K_n (R_n) are in good agreement with previous measurements for similar mobile surfaces and large bubbles [8–11].

We can also compare our measurements with those made on a single PB and where surface mobilities where deduced form the velocity profile [22]. In that work, a Poiseuille velocity profile was found for protein solutions, associated to a surface mobility M equal to 0.05, which is in agreement with the results of Figure 4. For SDS, an intermediate velocity profile, between a Poiseuille-like and a plug-like one, was observed, and a corresponding value of $M = 2$ was deduced. Figure 4a shows that $M = 2$ falls right into the intermediate regime, in agreement with these results.

Let us finally discuss the results obtained for both protein and SDS at bubble diameter $D < 0.5$ mm, which

do not fit with the above picture. As D decreases below 0.5 mm, we find that both K_c and K_n increase for the protein and SDS foams. For the casein foams, with $D =$ 0.45 mm, 0.3 mm and 0.18 mm, we found, respectively: $K_c = 10.1 \cdot 10^{-3}$, $K_c = 12.5 \cdot 10^{-3}$ and $K_c = 14.2 \cdot 10^{-3}$. For the SDS foams and with these same three bubble sizes, we found $K_n = 8.2 \cdot 10^{-3}$, $K_n = 9.6 \cdot 10^{-3}$ and $K_n = 13.1 \cdot 10^{-3}$. The exponent α remains close to 1/2 for the protein foams, while it decreases back to 1/3 for the SDS (Fig. 2). Thus, at small bubble sizes, the surface mobility appears to be high again. This is in agreement with other studies where this drainage regime has been found for small bubbles, with K_n equal to $9 \cdot 10^{-3}$ for $D = 0.2$ mm [27], in good agreement with our data. Obviously the increase in K_c can no longer be attributed to the variation of M (which decreases with decreasing bubble size). The surface parameter N increases with decreasing bubble size, and the bulk-surface coupling described by this parameter would lead to a trend similar to the one observed here. However, the calculated value of N is always too small to account for a drainage regime transition [21] ($N \sim 10^{-3}$ for our smallest bubbles). It is nevertheless striking to note that similar transitions have been observed in thin film drainage, occurring when $N \sim 10^{-5}$ [46,47]. When the films diameter become small (typically below 0.5 mm), the drainage becomes very fast, and dimples (instabilities leading to non-homogeneous film thickness, thicker in the center, thinner at the borders) are no longer observed [48]. This could change the hydrodynamic coupling between films and PBs, relaxing local pinches and the condition of zero surface velocity, allowing then the flow to evolve towards a plug flow.

6 Conclusion

The reported forced drainage experiments demonstrate that, over a very large range of experimental conditions, the relevant drainage control parameter is the mobility parameter M, which incorporates bubble size, liquid content and surface shear viscosity. Thanks to the large range of experimental conditions investigated here, a simple and consistent picture of foam drainage emerges: PBs and nodes can be considered as hydrodynamic resistors mounted in series, which resistances depend on the surface mobility. Foam drainage proceeds according to a balance between resistances in the PBs and in the nodes. We have found that a transition between drainage regimes occurs in an intermediate range of surface mobility, corresponding precisely to the point where the PBs and nodes resistance are equivalent. The self-consistency of the results first validates the usual assumptions made for modeling foam drainage —especially the classical picture of a liquid flow only through the network of PBs and nodes, with negligible transport in the thin films (also confirmed by recent numerical simulations [37])— and secondly, the geometrical constants used to describe PB and node geometries. We also show that drainage experiments can be used as a method for measuring surface shear viscosities. This drainage picture fails in the case of extremely small bubbles, where it is possible that another bulk-surface coupling, described by a parameter N, becomes important. Understanding this behavior and the role of the bulk viscosity [49] on the drainage transition (as it also appears in M and N), and determining the complete surface mobility dependence of the PBs and node resistances, remain important issues to be clarified for a complete understanding of foam drainage.

This work has been supported in part by the Centre National d'Etudes Spatiales (CNES) and the European Space Agency (ESA). YZ is grateful to Institut National de Recherche Agronomique (INRA) for a post-doctoral position. We have benefited from numerous stimulating discussions with D. Weaire, S. Cox, S. Hilgenfeldt and O. Pitois on drainage, and R. Douillard and V. Aguié-Béghin on the surface behavior of casein.

References

1. D. Weaire, S. Hutzler, *The Physics of Foams* (Oxford University Press, 1999).
2. D. Weaire, N. Pittet, S. Hutzler, D. Pardal, Phys. Rev. Lett. **71**, 2670 (1993).
3. G. Verbist, D. Weaire, Europhys. Lett. **26**, 631 (1994).
4. R. Phelan, D. Weaire, E.A.J.F. Peters, G. Verbist, J. Phys.: Condens. Matter **8**, L475 (1996).
5. G. Verbist, D. Weaire, A. Kraynik, J. Phys.: Condens. Matter **8**, 3715 (1996).
6. D. Weaire, S. Hutzler, G. Verbist, E.A.J. Peters, Adv. Chem. Phys., **102**, 315 (1997).
7. A. Saint-Jalmes, M.U. Vera, D.J. Durian, Eur. Phys. J. B **12**, 67 (1999).
8. S.A. Koehler, S. Hilgenfeldt, H.A. Stone, Phys. Rev. Lett. **82**, 4232 (1999)
9. M. Durand, G. Martinoty, D. Langevin, Phys. Rev. E **60**, R6307 (1999).
10. P.J. Wilde, A.R. Mackie, F.A. Husband, A.P. Gunning, V.J. Morris, A. Fillery-Travis, *Proceedings of the international Workshop on Foams and Films, Leuven, Belgium*, edited by D. Weaire, J. Banhart (MIT-Verlag, Bremen, 1999) p. 59.
11. S.A. Koehler, S. Hilgenfeldt, H.A. Stone, Langmuir **16**, 6327 (2000).
12. A. Saint-Jalmes, M.U. Vera, D.J. Durian, Europhys. Lett. **50**, 695 (2000).
13. S.A. Koehler, S. Hilgenfeldt, H.A. Stone, Europhys. Lett. **54**, 335 (2000).
14. S.J. Cox, D. Weaire, S. Hutzler, J. Murphy, R. Phelan, G. Verbist, Proc. R. Soc. London, Ser. A **456**, 2441 (2000).
15. S. Hutzler, D. Weaire, Philos. Mag. Lett. **80**, 419 (2000).
16. P. Grassia, J.J. Cilliers, S.J. Neethling, E. Ventura-Medina, Eur. Phys. J. E **6**, 325 (2001).
17. M. Safouane, M. Durand, A. Saint-Jalmes, D. Langevin, V. Bergeron, J. Phys. IV. **11**, 275 (2001) Pr6.
18. S.J. Cox, G. Bradley, S. Hutzler, D. Weaire, J. Phys.: Condens. Matter **13**, 4863 (2001).
19. S. Hilgenfeldt, S.A. Koehler, H.A. Stone, Phys. Rev.Lett. **86**, 4704 (2001).

20. S.J. Cox, G. Bradley, D. Weaire, Eur. Phys. J., Appl. Phys. **14**, 87 (2001).
21. M. Durand, D. Langevin, Eur. Phys. J. E **7**, 35 (2002).
22. S.A. Koehler, S. Hilgenfeldt, E.R. Weeks, H.A. Stone, Phys. Rev. E **66**, 040601(R) (2002).
23. A. Saint-Jalmes, D. Langevin, J. Phys.: Condens. Matter **14**, 9397 (2002).
24. P. Grassia, S.J. Neethling, J.J Cilliers, Eur. Phys. J. E **8**, 517 (2002).
25. V. Carrier, S. Destouesse, A. Colin, Phys. Rev. E. **65**, 1 (2002).
26. S.J Neethling, H.T. Lee, J.J. Cilliers, J. Phys.: Condens. Matter **14**, 331 (2002).
27. M.U. Vera, D.J. Durian, Phys. Rev. Lett. **88**, 088304-1 (2002).
28. D. Weaire, S. Hutzler, S. Cox, N. Kern, M.A. Alonso, W. Drenckhan, J. Phys.: Condens. Matter **15**, S65 (2003).
29. H.A. Stone, S.A. Koehler, S. Hilgenfeldt, M. Durand, J; Phys. Condens. Matter **15**, S283 (2003).
30. S.A. Koehler, S. Hilgenfeldt, E.R. Weeks, H.A. Stone, to be published in J. Colloid Interface Sci.
31. O. Pitois, C. Fritz, M. Adler, to be published in J. Colloid Interface Sci.
32. R.A. Leonard, R. Lemlich, AIChE J. **11**, 18 (1965).
33. A. Kraynik (1983) *Sandia Report* SAND 83-0844.
34. I.I. Gol'dfarb, K.B. Kann, I.R. Shreiber, Fluid Dyn. **23**, 244 (1988).
35. D. Desai, R. Kumar, Chem. Eng. Sci. **37**, 1361 (1982).
36. A. Nguyen, J. Colloid Interface Sci. **249**, 194 (2002)
37. S.A. Koehler, S. Hilgenfeldt, H.A. Stone, to be published in J. Colloid Interface Sci.
38. F.G. Gandolfo, H.L. Rosano, J. Colloid Interface Sci. **194**, 31 (1997).
39. P.A. Lemieux, M.U. Vera, D.J. Durian, Phys. Rev. E **57**, 4498 (1998).
40. M.U Vera, A. Saint-Jalmes, D.J Durian, Appl. Optics **40**, 4210 (2001).
41. S. Cox, private communication.
42. A. Aradian, E. Raphaël, P-G. de Gennes, Europhys. Lett. **55**, 834 (2001).
43. S. Hutzler, D. Weaire, R. Crawford, Europhys. Lett. **41**, 461 (1998).
44. M.U. Vera, A. Saint-Jalmes, D.J. Durian, Phys. Rev. Lett. **84**, 3001 (2001).
45. N.F. Djabbarah, D.T. Wasan, Chem. Eng. Sci. **37**, 175 (1982); J.T. Petkov, K.D. Danov, N.D. Denkov, R. Aust, F. Durst, Langmuir **12**, 2650 (1996); C. Barentin, C. Ybert, J.M. DiMeglio, J.F. Joanny, J. Fluid. Mech. **397**, 331 (1999).
46. G. Singh, G.J. Hirasaki, C.A. Miller, J. Colloid Interface Sci. **184**, 92 (1996).
47. S. Stoyanov, N. Denkov, Langmuir **17**, 1150 (2001).
48. O.D. Velev, G.N. Constantinides, D.G. Avraam, A.C. Payatakes, R.P. Borwankar, J. Colloid Interface Sci. **175**, 68 (1995).
49. M. Safouane, A. Saint-Jalmes, V. Bergeron, D. Langevin, submitted to Phys. Fluids.